PHYSICAL REVIEW D **93,** 094508 (2016)

Canonical approach to finite density QCD with multiple precision computation

Ryutaro Fukuda,[1,2] Atsushi Nakamura,[3,4,5] and Shotaro Oka[6]

[1]*Department of Physics, The University of Tokyo,7-3-1 Hongo, Bunkyo-ku, Tokyo 113-0033, Japan*
[2]*Institute für Theoretische Physik, ETH Zürich, CH-8093 Zürich, Switzerland*
[3]*Research Center for Nuclear Physics, Osaka University, Ibaraki 567-0047, Japan*
[4]*Theoretical Research Division, Nishina Center, RIKEN, Wako 351-0198, Japan*
[5]*School of Biomedicine, Far Eastern Federal University, Vladivostok 690950, Russia*
[6]*Department of Physics, Rikkyo University, 3-34-1 Nishi-Ikebukuro, Toshima-ku, Tokyo 171-8501, Japan*

(Received 4 May 2015; published 24 May 2016)

In this study, we calculated the dependence of thermodynamic observables, namely, pressure, baryon number density, and baryon susceptibility, on the baryon chemical potential μ_B through lattice quantum chromodynamics using the canonical approach. We compare the results with those obtained using the multiparameter reweighting (MPR) method. The results of these methods were found to be in very good agreement in the regions where the errors of the MPR method are under control. The canonical method yields reliable results up to $\mu_B/T = 3$, where T is the temperature. Multiple precision operations play important roles in the evaluation of canonical partition functions.

DOI: 10.1103/PhysRevD.93.094508

I. INTRODUCTION

Quantum chromodynamics (QCD) is the fundamental theory describing strong interactions. It is well known that QCD has a rich phase structure at finite temperature and density values [1]. However, regions that can be accessed with QCD perturbation theory are limited. Currently, the most promising method to explore phase diagrams is through a lattice QCD simulation, which is a first-principles calculation.

Although lattice QCD simulations are very helpful in analyses of the phase diagram of a finite temperature system, at finite density they suffer a severe problem called the sign problem, and the results of the first-principles calculation are available only within a small chemical potential range. In finite temperature and density systems, numerous physically interesting targets such as the early Universe, neutron stars, and quark matter, have yet to be explored. Therefore, it is important to explore methods of investigating finite-density QCD systems from *ab initio* calculations; this is an urgent subject in the fields of particle and nuclear physics.

The canonical approach [2] we study in this paper is a promising candidate for this purpose. In Ref. [3], a fugacity expansion was constructed as a winding number expansion by the hopping parameter expansion method, and the chiral condensate and thermodynamic quantities were studied. A more detailed analysis was performed in Ref. [4] for a wide range of temperatures and chemical potentials. In contrast with these studies, we address two questions in this work:

(1) Does the canonical approach to lattice QCD produce results consistent with results of multiparameter reweighting (MPR) [5] and Taylor expansion [6]?
(2) When obtaining the canonical partition functions for a large baryon number, what are the roles of the multiple precision calculations?

As explained in detail later, in this work we adopt a winding number expansion [7–9] for Wilson fermions based on the hopping parameter expansion. The major advantage of this method is to be able to reduce numerical costs for calculations of fermion determinants as stated in Appendix A, and this merit is crucial for our work. This is because in the canonical approach we have to calculate a lot of fermion determinants at a variety of values of pure imaginary chemical potentials to calculate canonical partition functions. Numerical costs in the case of using an exact formula are expensive even if we adopt a kind of reduction formula for Wilson fermions (see, e.g., [10–13]). Therefore, in this instance, it is hard to adopt a sufficiently large lattice size considering recent computational resources. Moreover, the main aim of this work is to investigate if the canonical approach works well with our strategy. This trial can provide us suggestive information because it is reported that the canonical approach has several numerical instabilities [8]. Taking these circumstances into consideration, it can be a suitable choice for this work to adopt the winding number expansion for realizing simple and meaningful numerical analyses as a kind of test.

II. FRAME WORK

A. Basic concept of canonical approach in QCD

For N_f-flavor QCD with degenerate quark masses, the grand canonical partition function at a finite temperature T and a finite quark chemical potential μ_q is given by the path integral formulation as

$$Z_{GC}(T,\mu_q) = \int d[U]\{\det\Delta(\mu_q)\}^{N_f} e^{-S_g}, \quad (1)$$

where $\det\Delta(\mu_q)$ is a one-flavor fermion determinant and S_g is a gauge action. Because the fermion determinant has the property

$$[\det\Delta(\mu_q)]^* = \det\Delta(-\mu_q^*), \quad (2)$$

the Monte Carlo measure $\{\det\Delta(\mu_q)\}^{N_f} e^{-S_g}$ becomes complex at a finite real chemical potential, and the standard Monte Carlo method breaks down. Consequently, we cannot study finite density thermodynamics with the standard grand canonical method. This difficulty is usually called the sign problem [14,15].

A system described by the grand canonical partition function $Z_{GC}(T,\mu_q)$ is equivalent to a system described by the canonical partition function $Z_C(n,T)$ with a fugacity $e^{\mu_q/T}$ in a thermodynamic limit. The relationship between the two ensembles can be written as a fugacity expansion [13] using the eigenvectors $|n\rangle$ of the number operator $\hat{N}$ ($\hat{N}|n\rangle = n|n\rangle$),

$$\begin{aligned} Z_{GC}(T,\mu_q) &= \mathrm{Tr} e^{-(\hat{H}-\mu_q\hat{N})/T} \\ &= \sum_{n=-\infty}^{\infty} \langle n|e^{-\hat{H}/T}|n\rangle e^{n\mu_q/T} \\ &\equiv \sum_{n=-\infty}^{\infty} Z_C(n,T) e^{n\mu_q/T}. \end{aligned} \quad (3)$$

If we obtain the canonical partition function $Z_C(n,T)$ for each net quark number n, we can construct the grand canonical partition function as a polynomial of the fugacity with coefficients Z_C. The Lee-Yang zeros [16], which reflect a critical nature of a thermodynamic system [17], can also be obtained from this formula.

The canonical partition functions are constructed through the Fourier transformation of the grand canonical partition function at a pure imaginary chemical potential [2]:

$$Z_C(n,T) = \frac{1}{2\pi}\int_0^{2\pi} d\left(\frac{\mu_I}{T}\right) Z_{GC}\left(\frac{i\mu_I}{T}\right) e^{-in\mu_I/T}, \quad (4)$$

where $\mu_I \in \mathbb{R}$. Eq. (2) demonstrates that the fermion determinant is real in the case of a pure imaginary chemical potential. Monte Carlo simulations can then be performed, and the canonical partition functions can be obtained from Eq. (4). Equation (4) also requires that the canonical partition functions are real because the grand canonical partition function is an even function (charge conjugation invariant) in terms of a chemical potential.

Once the canonical partition functions Z_C are determined, the grand partition function can be constructed using Eq. (3) for any *real* quark chemical potential. This is because the chemical potential dependence of the grand canonical partition function Z_{GC} in Eq. (3) appears only in a fugacity $e^{\mu_q/T}$, which is the polynomial variable, and not in the coefficients Z_C. An effect of a chemical potential on the grand canonical partition function appears through the fugacity, and the canonical partition functions simply play the role of coefficients in the fugacity expansion of the grand canonical partition function.

B. Winding number expansion of grand canonical partition function

In this work, we employ the renormalization group (RG)-improved gauge action [18]

$$S_g = \frac{\beta}{3}\left[c_0 \sum_{n,\mu<\nu} \mathrm{Tr} P_{\mu,\nu}(n) + c_1 \sum_{n,\mu<\nu} \mathrm{Tr} R_{\mu,\nu}(n)\right], \quad (5)$$

$$P_{\mu,\nu}(n) = U_\mu(n) U_\nu(n+\hat{\mu}) U_\mu^\dagger(n+\hat{\nu}) U_\nu^\dagger(n), \quad (6)$$

$$\begin{aligned} R_{\mu,\nu}(n) = {} & U_\mu(n) U_\mu(n+\hat{\mu}) U_\nu(n+2\hat{\mu}) \\ & \times U_\mu^\dagger(n+\hat{\mu}+\hat{\nu}) U_\mu^\dagger(n+\hat{\nu}) U_\nu^\dagger(n), \end{aligned} \quad (7)$$

with the effective coupling constant $\beta = 6/g^2$ defined using the gauge coupling constant g, $c_1 = -0.331$, and $c_0 = 1 - 8c_1$, and the clover improved Wilson fermion action [19] with the quark matrix

$$\begin{aligned} \Delta(n,m,\mu_q) = {} & \delta_{nm} - \kappa C_{SW}\delta_{nm}\sum_{\mu\le\nu}\sigma_{\mu\nu}F_{\mu\nu}(n) - \kappa\sum_{i=1}^{3}[(1-\gamma_i)U_i(n)\delta_{m,n+\hat{i}} + (1+\gamma_i)U_i^\dagger(m)\delta_{m,n-\hat{i}}] \\ & - \kappa[e^{+\mu_q a}(1-\gamma_4)U_4(n)\delta_{m,n+\hat{4}} + e^{-\mu_q a}(1+\gamma_4)U_4^\dagger(m)\delta_{m,n-\hat{4}}] \equiv 1 - \kappa Q(\mu_q). \\ F_{\mu\nu}(n) = {} & P_{\mu,\nu}(n) + P_{\nu,-\mu}(n) + P_{-\mu,-\nu}(n) + P_{-\nu,\mu}(n) \end{aligned} \quad (8)$$

Here, n and m are space-time coordinates on a lattice; κ is the hopping parameter; and μ_q is a quark chemical potential, which is introduced to the temporal part of the link variables. Also, $\sigma_{\mu\nu}$ is defined as $\sigma_{\mu\nu} = i[\gamma_\mu,\gamma_\nu]/2$.

To obtain the canonical partition functions, the grand canonical partition functions must be computed at various pure imaginary chemical potential values using the Fourier transformation in Eq. (4).

We use a reweighting method to evaluate the grand canonical partition function,

$$Z_{GC}(i\mu_I) = \int d[U]\left[\frac{\det\Delta(i\mu_I)}{\det\Delta(\mu_0)}\right]^{N_f}\{\det\Delta(\mu_0)\}^{N_f}e^{-S_g} = \left\langle\left[\frac{\det\Delta(i\mu_I)}{\det\Delta(\mu_0)}\right]^{N_f}\right\rangle_{\mu_0} Z_{GC}(\mu_0), \quad (9)$$

where $\mu_0 = 0$ or pure imaginary values. We can then evaluate the canonical partition function as

$$\frac{Z_C(n,T)}{Z_{GC}(T,\mu_0)} = \frac{1}{2\pi}\int_0^{2\pi} d\theta\left\langle\left[\frac{\det\Delta(i\theta)}{\det\Delta(\mu_0)}\right]^{N_f}\right\rangle_{\mu_0} e^{-in\theta}. \quad (10)$$

Now, the evaluation of the grand canonical partition function is reduced to the calculation of ratios of fermion determinants in Eq. (9).

In this work, we adopt a winding number expansion [8] to calculate the fermion determinant assuming that the hopping parameter is small enough. Therefore, our starting point is the hopping parameter expansion on a logarithm of a fermion determinant as follows:

$$\log\det\Delta(i\mu_I) = \mathrm{Tr}\log\{1-\kappa Q(i\mu_I)\} = -\sum_{n=1}^{\infty}\frac{\kappa^n}{n}\mathrm{Tr}Q^n(i\mu_I). \quad (11)$$

The trace in Eq. (11) is taken over space-time, spinor, and color indices.

Taking into account a feature of the trace in terms of space-time indices in Eq. (11), we can easily find that all nonzero contribution of the trace in Eq. (11) comes from closed loops on a lattice. Moreover, the chemical potential dependence comes only from closed loops which are winding along positive or negative time directions through an antiperiodic boundary condition considering an introduction of the quark chemical potential in Eq. (8). For example, the trace of a closed loop which is winding along a positive time direction n times can be evaluated as $Ce^{in\mu_I N_t a} = Ce^{in\mu_I/T}$, where C is a complex constant. Therefore, if we classify all closed loops in Eq. (11) according to the "winding number," which is the number of net windings along the time direction, as a result, we can reach the following expression with complex coefficients W_n and the complex fugacity $e^{i\mu_I/T}$, where n represents the winding number:

$$\log\det\Delta(i\mu_I) = \sum_{n=-\infty}^{\infty} W_n e^{in\mu_I/T}. \quad (12)$$

Negative values of the winding number n in Eq. (12) stand for winding numbers of loops along a negative time direction. A notable fact is that the coefficient W_n has no chemical potential dependence at all, and the chemical potential dependence appears only in the complex fugacity. This means that we have only to calculate W_n with gauge configurations given at one chemical potential value and then using the set of W_n we can evaluate fermion determinants at all desired chemical potential values tuning a chemical potential in the fugacity.

C. Constraint on canonical partition function from symmetry of QCD

Roberge and Weiss noted that the QCD grand canonical partition function at a pure imaginary chemical potential has the following periodicity [20]:

$$Z_{GC}\left(\frac{i\mu_I}{T}\right) = Z_{GC}\left(\frac{i\mu_I}{T}+\frac{2\pi ik}{3}\right), \quad (13)$$

where $k \in \mathbb{N}$. Using Eq. (13), we rewrite the grand canonical partition function as

$$Z_{GC}\left(\frac{i\mu_I}{T}\right) = \frac{1}{3}\sum_{k=0}^{2} Z_{GC}\left(\frac{i\mu_I}{T}+\frac{2\pi ik}{3}\right). \quad (14)$$

We then obtain the relation

$$Z_C(n,T) = \frac{1}{2\pi}\int_0^{2\pi} d\left(\frac{\mu_I}{T}\right) Z_{GC}\left(\frac{i\mu_I}{T}\right)e^{-in\mu_I/T} \times\left[\frac{1+e^{i\frac{2\pi}{3}n}+e^{i\frac{4\pi}{3}n}}{3}\right] \quad (15)$$

and the following important constraint on the canonical partition functions [2,20,21]:

$$Z_C(n\neq 3k) = 0. \quad (16)$$

Note that this constraint holds true in both the confining and the deconfining phases.

Thus, the grand canonical partition function can be written as

$$Z_{GC}(T,\mu_B) = \sum_{B=-\infty}^{\infty} Z_C(B,T)e^{B\mu_B/T}, \quad (17)$$

where $B \in \mathbb{N}$. Because the quantum number B can be interpreted as a net baryon number, μ_B can be regarded as a baryon chemical potential, which is related to a quark chemical potential as $\mu_B = 3\mu_q$.

D. Thermodynamic observables

In a homogeneous system, a dimensionless equation of state at (μ_B, T) is given by

$$\frac{p(\mu_B,T)}{T^4} = \frac{1}{V_s T^3}\log Z_{GC}(\mu_B,T) = \left(\frac{N_t}{N_s}\right)^3 \log Z_{GC}(\mu_B,T), \quad (18)$$

where V_s is the three-dimensional spatial volume of a lattice, $N_s = N_x = N_y = N_z$, and $T^{-1} = N_t a$ for a lattice spacing of a. A deviation of the pressure from $\mu_B = 0$ is given by

$$\frac{\Delta p(\mu_B,T)}{T^4} = \frac{p(\mu_B,T)}{T^4} - \frac{p(0,T)}{T^4} = \left(\frac{N_t}{N_s}\right)^3 \log\left(\frac{Z_{GC}(\mu_B,T)}{Z_{GC}(0,T)}\right). \quad (19)$$

A dimensionless baryon number density n_B/T^3 and a baryon susceptibility χ/T^2 are

$$\frac{n_B(\mu_B,T)}{T^3} = \frac{\partial}{\partial(\mu_B/T)}\frac{p(\mu_B,T)}{T^4}, \quad (20)$$

$$\frac{\chi(\mu_B,T)}{T^2} = \frac{\partial^2}{\partial(\mu_B/T)^2}\frac{p(\mu_B,T)}{T^4}. \quad (21)$$

III. NUMERICAL RESULTS

A. Lattice design

We adopted the two-flavor clover-improved Wilson fermion action with $C_{\rm SW} = (1 - 0.8412/\beta)^{-3/4}$ evaluated by a one-loop perturbation theory and the RG–improved gauge action. All simulations were performed on a $N_x \times N_y \times N_z \times N_t = 8 \times 8 \times 8 \times 4$ lattice. We considered values of $\beta = 2.00$, 1.95, 1.90, 1.85, 1.80, and 1.70, which correspond to $T/T_c = 1.35(7)$, 1.20(6), 1.08(5), 0.99(5), 0.93(5), and 0.84(4), respectively. The values of the hopping parameter κ were determined for each value of β by following the line of constant physics for the case of $m_\pi/m_\rho = 0.8$, as in Ref. [22].

We generated gauge configurations at $\mu_0 = 0$ using the hybrid Monte Carlo (HMC) method. The step size $d\tau$ and number of steps N_τ of HMC were set to $d\tau = 0.02$ and $N_\tau = 50$ so that the simulation time was $d\tau \times N_\tau = 1$. After the first 2000 trajectories for thermalization, for every 200 trajectories we adopted 400 configurations for each parameter set.

B. Solution to eliminate instability of Fourier transformation in the canonical approach

Before proceeding to our numerical results, in this subsection, we discuss an instability of a use of Fourier transformations in the canonical approach and our strategy to eliminate it.

Because the fugacity expansion of the grand canonical partition function given in Eq. (3) converges at a real baryon chemical potential, the canonical partition function $Z_C(n,T)$ must decrease when the absolute value of a net baryon number n increases. This means that we have to work with very small values in the Fourier transformation. This step is quite difficult from the viewpoint of numerical calculations because the Fourier transformation is an oscillatory integral.

1. Instability of Fourier transformation

In a numerical calculation, the Fourier transformation given in Eq. (4) is computed by the discrete Fourier transform (DFT) as

$$Z_C(n,T) = \frac{1}{N}\sum_{k=0}^{N-1} Z_{GC}\left(i\frac{\mu_I}{T} = i\frac{2\pi k}{N}\right) e^{i\frac{2\pi k}{N}n}, \quad (22)$$

where N is an interval number of the DFT. Because the DFT is simply a discretized version of the Fourier transform in a continuum theory, the instability of the DFT in the canonical approach is caused by numerical errors, the types of which are classified as rounding error, truncation error, cancellation of significant digits, and loss of trailing digits. The instability of the DFT does not arise from truncation error because the DFT is not an infinite series. Accordingly, it is natural to consider that the instability originates from the cancellation of significant digits, the loss of trailing digits, or both. In this work, we actually monitored the behavior of all variables in our DFT program to study the

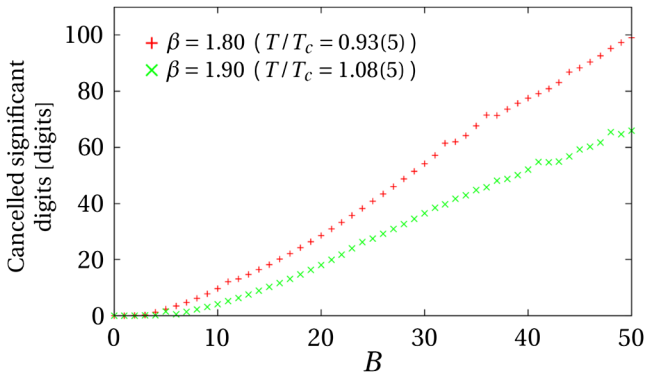

FIG. 1. Canceled significant digits in the DFT calculations at temperatures above (upper red points) and below (lower green points) T_c.

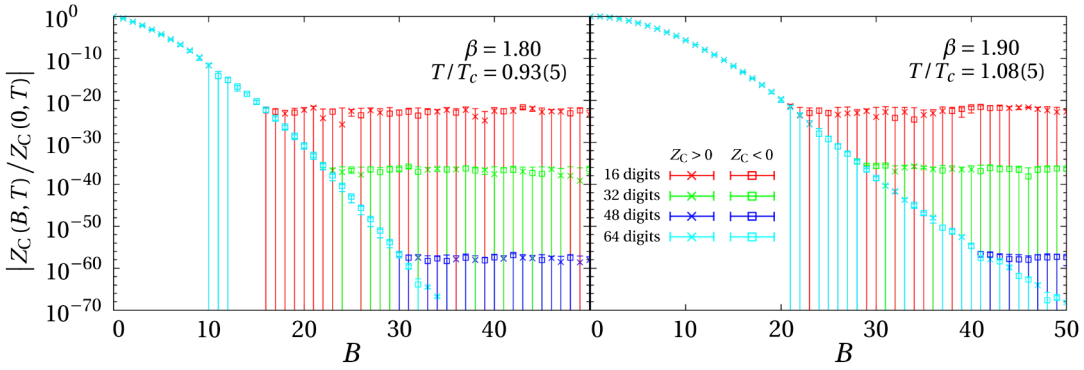

FIG. 2. Relationship between the behavior of $Z_C(B,T)$ and the precision of the variables in the DFT at temperatures above (right) and below (left) T_c. Both include 16 (double precision, upper red points), 32 (second green points), 48 (third blue points), and 64 (lowest cyan points) significant figures. Errors are estimated by the Jackknife method.

effects of these two errors. As a result, we found that the cancellation of significant digits is not negligible in the DFT program. Figure 1 shows canceled digits in our DFT program. For example, 80 digits are canceled in the case where $\beta = 1.80$ and $B = n/3 = 40$. We also found that the occurrence of the cancellation does not depend on temperatures of our system.

2. Solution to eliminate instability by multiple precision calculation

A cancellation of significant digits occurs in the following type of calculation:

$$1.234567 - 1.234566 = 0.000001$$
$$(7\,\text{significant digits}) \quad (1\,\text{significant digit}). \tag{23}$$

In this case, six significant digits are lost.

To reduce the effect of this cancellation, the number of significant digits should be increased. Let us consider the following calculation with 22 significant digits:

$$1.234567444444444444444 - 1.234566111111111111111$$
$$(22\,\text{significant digits})$$
$$= 0.000001333333333333333(16\,\text{significant digits}). \tag{24}$$

Although six significant digits are still lost in this calculation, 16 significant digits remain in the final result.

Summarizing the above process, precision of a calculation result can be retained by increasing the number of significant digits of input variables in this way. Figure 2 shows the effect of canceled digits in the calculation of $Z_C(B,T)$ with 16, 32, 48, and 64 significant digits. According to this figure, when evaluating $Z_C(B,T)$ for a large baryon number B, it is essential to increase the number of significant digits of the variables in the DFT.

C. Thermodynamic observables at finite real baryon chemical potential

1. Calculation procedure

First, the coefficients of the winding number expansion W_n in Eq. (12) were approximately computed up to $n = 120$ using the hopping parameter expansion up to the $120N_t$-th order in Eq. (11) with 400 configurations in all temperature cases. Detailed numerical algorithm to calculate a set of W_n making use of the hopping parameter expansion is explained in Ref. [23]. We used 64 and 128 noise vectors for temperatures above and below T_c, respectively, to calculate the trace in the fermion determinant given in Eq. (11). Validity of the noise method for the trace is briefly discussed in Appendix B. We then evaluated the grand canonical partition functions at various pure imaginary chemical potentials using the winding number expansion with sets of $\{W_n\}$. After that, we evaluated the canonical partition function through the Fourier transformation and thermodynamic observables. Except in a generation of gauge configurations and a calculation of W_n, a multiple precision calculation [24] was adopted with 400 significant digits to ensure sufficient precision. Gauge configurations and sets of W_n were computed with double precision, i.e., approximately 16 significant digits.

In general, the canonical partition functions can be obtained as a complex number in numerical calculations because of the numerical errors. Therefore, we adopt only the real part of the canonical partition function. If the first time the real part of the canonical partition function is negative is at a baryon number of n_B, the results up to $n_B - 1$ are adopted as reliable canonical partition functions.

In the following section, we compare our canonical results with MPR results in Ref. [13] adopting the same numerical setup as Ref. [13].

In the MPR method, an expectation value of an observable O at a finite chemical potential can be calculated as

$$\langle O(\mu)\rangle = \frac{1}{Z_{GC}(\mu)}\int [dU]\left(O(\mu)\frac{\det\Delta(\mu)}{\det\Delta(0)}e^{-(\beta-\beta_0)S_g}\right) \times \det\Delta(0)e^{-\beta_0 S_g} = \frac{\langle O(\mu)\frac{\det\Delta(\mu)}{\det\Delta(0)}e^{-(\beta-\beta_0)S_g}\rangle_0}{\langle\frac{\det\Delta(\mu)}{\det\Delta(0)}e^{-(\beta-\beta_0)S_g}\rangle_0}, \quad (25)$$

where $\langle\cdots\rangle_0$ stands for an average with configurations generated at $(\beta_0, \mu = 0)$. This procedure helps us to improve the overlap problem in the importance sampling at finite density, and we can get better signals. Nowadays, it is found that the MPR method is valid for a low density system, and this method is frequently used for analyzing such a system.

In Ref. [13], the authors also discussed the consistency between the MPR and Taylor expansion methods with Wilson-clover fermions and concluded that both methods produced consistent results in a small chemical potential region where errors of both methods could be under control. Therefore, our work enables us to check consistency among our canonical approach, MPR method, and Taylor expansion method.

2. Estimation of truncation error in fugacity expansion

In our numerical calculations, the fugacity expansion of the grand canonical partition function must be considered as a finite series

$$Z_{GC}(T,\mu_B) = \sum_{B=-N_{\max}}^{N_{\max}} Z_C(B,T)e^{B\mu_B/T}. \quad (26)$$

Therefore, we have to judge the baryon chemical potential region in which the results are free from truncation error. There may be several possible methods of analyzing the effect of the truncation error; the method used in this study is as follows.

First, we evaluate expectation values $\langle O(\mu_B)\rangle_{N_{\max}}$ of a thermodynamic observable using Eq. (26). Next, we calculate expectation values $\langle O(\mu_B)\rangle_{N_{\max}-1}$ by subtracting 1 from $N_{\max}$ in Eq. (26). We then evaluate the relative error $R_{\rm ob}(\mu_B)$ from these expectation values as

$$R_{\rm ob}(\mu_B) \equiv 1 - \frac{\langle O\rangle_{N_{\max}-1}}{\langle O\rangle_{N_{\max}}} < 10^{-3}. \quad (27)$$

In this study, we consider the expectation values to be reliable if the relative error is less than 10^{-3}. Using this approach, we can ensure that the expectation values of the thermodynamic observables in the baryon chemical potential region determined by the above analysis method have at least two significant digits against the truncation error.

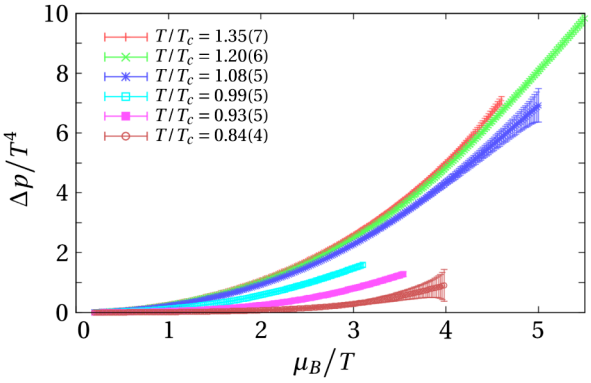

FIG. 3. Chemical potential dependence of pressure. The red, green, blue, cyan, magenta, and brown points are the results at $T/T_c = 1.35$, 1.20, 1.08, 0.99, 0.93, and 0.83, respectively. The upper bound of the baryon chemical potential is determined by Eq. (27).

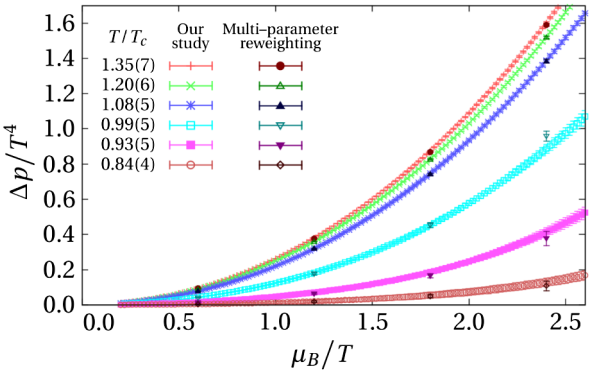

FIG. 4. Comparison of pressure calculated by the canonical approach and the MPR method. The colors of the data points are the same as in Fig. 3 with some additional colors. The data points plotted in the additional colors of dark red, dark green, dark blue, dark cyan, dark magenta, and dark brown points are the results at $T/T_c = 1.35$, 1.20, 1.08, 0.99, 0.93, and 0.83, respectively, as calculated by the MPR method.

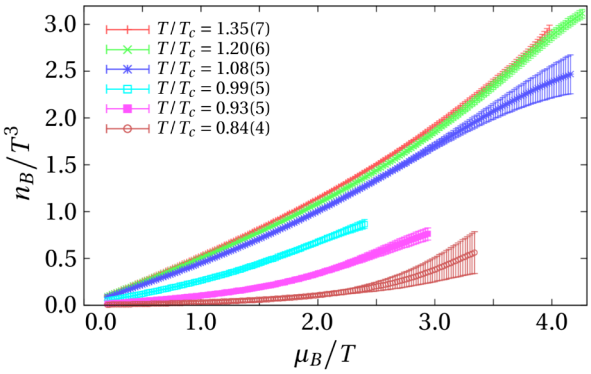

FIG. 5. Chemical potential dependence of baryon number density. The colors of the data points are the same as in Fig. 3. The upper bound of the baryon chemical potential is determined by Eq. (27).

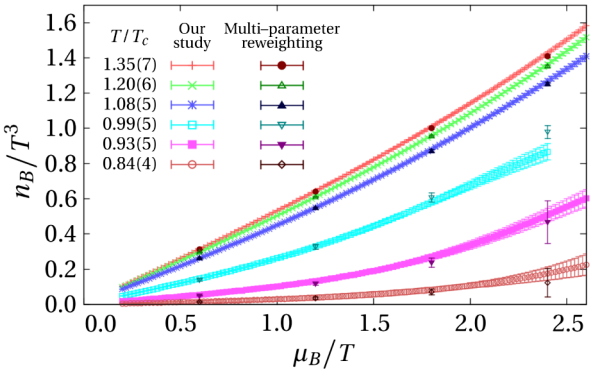

FIG. 6. Comparison of the baryon number densities calculated by the canonical approach and the MPR method. The colors of the data points are the same as in Fig. 4.

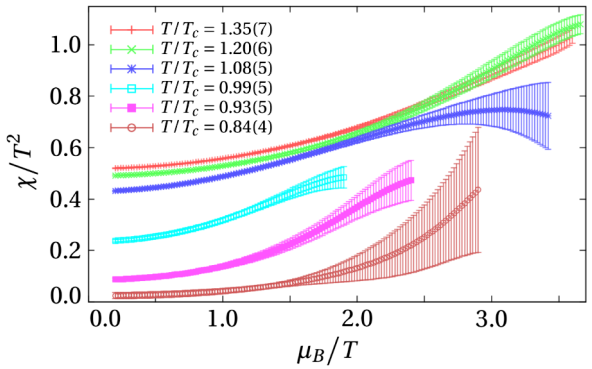

FIG. 7. Chemical potential dependence of baryon susceptibility. The colors of the data points are the same as in Fig. 3. The upper bound of the baryon chemical potential is determined by Eq. (27).

3. Thermodynamic observables

Using the error estimation method described in the previous subsection, we analyze the chemical potential dependence of the thermodynamic observables and study the validity range of our canonical approach. First, we examine the pressure. Figure 3 shows that the pressure results at temperatures above T_c do not suffer from large errors up to a ratio μ_B/T of approximately 5, and the results at temperatures below T_c are reliable up to a ratio μ_B/T of approximately 3.5–4. Conversely, the results at temperatures just below T_c are reliable only up to a ratio μ_B/T of approximately 3. This may be because we generated configurations at $\mu_0 = 0$, and they suffered from fluctuations caused by the phase transition at zero density. We may obtain clearer signals if we generate configurations at pure imaginary chemical potentials because T_c at a pure imaginary chemical potential is higher than T_c at a zero chemical potential. Figure 4 shows that the pressure calculated by the canonical approach is consistent with the pressure results obtained using MPR method.

Next, we consider the expectation value of the baryon number density. Figure 5 demonstrates that for temperatures above and below T_c, the results are reliable up to ratios μ_B/T of approximately 4 and 3–3.5, respectively, whereas the reliable baryon chemical potential range of the results for temperatures just below T_c are limited for ratios μ_B/T of up to 2.4. This may be for the same reason described in the pressure analysis.

Figure 6 demonstrates good agreement between the results of the canonical approach and those of the MPR method in the baryon number density case. Moreover, the gradient of the baryon number density n_B/T^3 as a function of a baryon chemical potential becomes smaller as the temperature decreases. In a zero temperature case, n_B is expected to be zero up to $\mu_B/T = m_B/T$, where m_B is the lightest baryon mass of a system, and becomes a finite value at this point. The data at $T/T_c = 0.84$ in Fig. 5 does in fact show such a feature.

Finally, we investigate the baryon susceptibility. Figure 7 shows that the results at temperatures above T_c are reliable up to a ratio μ_B/T of approximately 3.5, whereas those at temperatures below T_c are reliable up to $T_c = 2.4 - 2.9$. From Fig. 8, we find that the susceptibility results of the canonical approach are in very good agreement with those

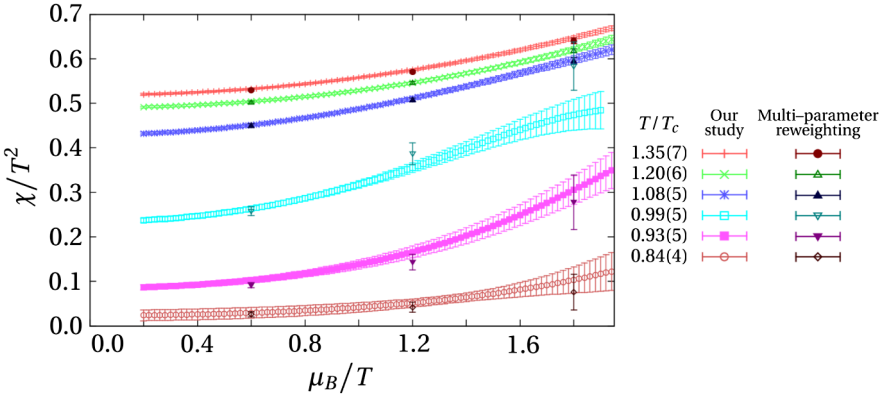

FIG. 8. Comparison of baryon susceptibilities calculated by the canonical approach and the MPR method. The colors of the data points are the same as in Fig. 4.

of the MPR method. The baryon susceptibility as a function of the ratio μ_B/T does not show a clear peak, and thus, signals of the transition between the confining and deconfining phases at finite density cannot yet be observed.

IV. SUMMARY AND OUTLOOK

In this paper, the canonical approach was shown to be consistent with the MPR method. Moreover, the canonical approach provides reliable results beyond $\mu_B/T = 3$ for almost all observables. This is very encouraging for the first-principles calculation of finite density QCD because other methods, such as MPR, Taylor expansion, and imaginary chemical potential [25], yield reliable information in practical situations only up to $\mu_B/T = 3$. A multiple precision calculation contributes to this conclusion.

Getting more reliable signals of thermodynamic quantities in a large baryon chemical potential region, we need to calculate the canonical partition functions more accurately at large baryon numbers. As shown in Fig. 2, our canonical partition functions currently have inadequate phases at some baryon numbers, although these should have a real positive value in principle. Considering the errors determined by the Jackknife analysis, we can conclude that these phases are not caused by the statistical error. In our opinion, this may originate in the overlap problem [14]. In this work, we calculate the grand canonical partition functions at all pure imaginary chemical potential with gauge configurations generated at zero chemical potential through the simplest reweighting method. However, practically speaking, we have to calculate them with gauge configurations generated at suitable pure imaginary chemical potentials to realize the appropriate importance sampling. This point is a lack of our work, and we need to improve it next time.

The canonical approach has been investigated in several previous studies [2,8,21,26–30]. We can also find through our work that it is a useful and promising method; however, our method may be improved further to obtain results under more realistic conditions, i.e., lighter quark mass, larger volume, finer lattice spacing, and higher density. Although the hopping parameter expansion yielded very interesting results in this study, the next step is to calculate the fermion determinant without this approximation; we have learned from this study that the key point is to calculate the determinant at imaginary chemical potential values that can undergo the Fourier transformation with high accuracy in Eq. (4). This requires more computational resources than what has been reported here but is within the scope of the next-generation high-performance era.

ACKNOWLEDGMENTS

This study was conducted for Zn Collaboration. We would like to thank the members of Zn Collaboration, S. Sakai, A. Suzuki, and Y. Taniguchi for their powerful support. We appreciate the useful discussions we had with K. Fukushima and Ph. de Forcrand. R. F. thanks the Yukawa Institute for Theoretical Physics, Kyoto University. Discussions during the YITP workshop YITP-T-14-03 on "Hadrons and Hadron Interactions in QCD" were useful in the completion of this work. R. F. also would like to thank ETH Zürich for its warm hospitality. S. O. thanks T. Eguchi for his valuable discussions and encouragement. This work is supported in part by Grants-in-Aid from the Ministry of Education (No. 15H03663 and No. 26610072). These calculations were performed with SX-9 and SX-ACE at the Research Center for Nuclear Physics (Osaka) and SR16000 at the Yukawa Institute for Theoretical Physics (Kyoto).

APPENDIX A: WINDING NUMBER EXPANSION

In this appendix, we summarize essential features to construct the winding number expansion. An algorithm to compute these steps are described in [23].

(i) fermion matrix: $\Delta(\mu) = \mathrm{I} - \kappa Q(\mu)$.

(ii) $\log\det\Delta = \mathrm{Tr}\log(1-\kappa Q) = -\sum_k \frac{1}{k}\kappa^k \mathrm{Tr}Q^k$.

(iii) All of Q^k makes lines, but only closed lines remain in $\mathrm{Tr}Q^k$.

(iv) Wilson loops have no μ dependence (Loop W in Fig. 9).

(v) Only loops which wind along the t direction have μ dependence: $\exp(\pm k\mu a N_t) = (\exp(\mu/T))^{\pm k}$ (Loop P1 and P2 in Fig. 9).

(vi) In calculating $\mathrm{Tr}Q^k$, we use the noise method,

$$\mathrm{Tr}Q^k = \sum_{a,\alpha,x}\langle a,\alpha,x|Q^k|a,\alpha,x\rangle \sim \frac{1}{N_{\mathrm{noise}}}\sum_{r=1}^{N_{\mathrm{noise}}}\langle\eta^{(r)}|Q^k|\eta^{(r)}\rangle,$$

where a, α, and x are color, spinor, and coordinate indices, respectively. Here, η^l are random numbers which satisfy

$$\frac{1}{N_{\mathrm{noise}}}\sum_r(\eta^{(r)}_{a,\alpha,x})^*\eta^{(r)}_{b,\beta,y} = \delta_{a,b}\delta_{\alpha,\beta}\delta_{x,y},$$

as $N_{\mathrm{noise}} \to \infty$.

(vii) Then, we construct $\det\Delta$ from these W_n,

$$\det\Delta = \exp\left(\sum_{n=-N_{\mathrm{max}}}^{N_{\mathrm{max}}} W_n\xi^n\right), \tag{A1}$$

where $\xi \equiv \exp(\mu/T)$.

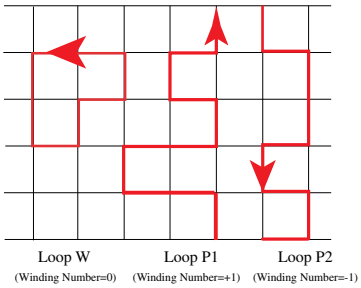

FIG. 9. Calculation of winding number coefficients, W_n: Schematical overview.

APPENDIX B: COMPLEXITY OF REDUCTION FORMULA AND WINDING NUMBER EXPANSION FOR FERMION DETERMINANT

To come right to the point, time complexities for the reduction formula [16] and the winding number expansion can be estimated to $O((N_xN_yN_z)^3 \times N_t)$ and $O(N_xN_yN_z \times N_t^3)$, respectively. Therefore, in an actual finite temperature-density system, numerical cost for the reduction formula is much higher than the winding number expansion in a large lattice. Moreover, the reduction formula needs much main memory because eigenvalues of a large-scale dense matrix must be calculated directly. In the reduction formula, first of all, we construct $4N_cN_xN_yN_z \times 4N_cN_xN_yN_z$ matrices $\alpha(t_i)$, $\beta(t_i)$ on each time slice from the original fermion matrix Δ whose rank is $N = 4N_cN_xN_yN_zN_t$, where N_c is the number of color degrees of freedom. The fermion determinant can be calculated using these matrices as follows:

$$\det\Delta(\mu) = e^{\mu N/2}\left(\prod_{i=1}^{N_t}\det\alpha(t_i)\right)\det\left(e^{-\mu/T}+Q\right), \tag{B1}$$

$$Q = \prod_{i=1}^{N_t}\alpha^{-1}(t_i)\beta(t_i). \tag{B2}$$

We need to calculate eigenvalues of Q to obtain the fermion determinant as the following form of a fugacity expansion:

$$\det\Delta(\mu) = \sum_{n=-4N_cN_xN_yN_z/2}^{4N_cN_xN_yN_z/2} C_n e^{n\mu/T}. \tag{B3}$$

The matrix Q is a dense matrix because it includes inverse matrices of $\alpha(t_i)$. Consequently, we need main memory of approximately $(4N_cN_xN_yN_z)^2 \times 16$ bytes at least in case of a double precision calculation. This procedure also hinders us a numerical simulation on the large size of a lattice at this stage.

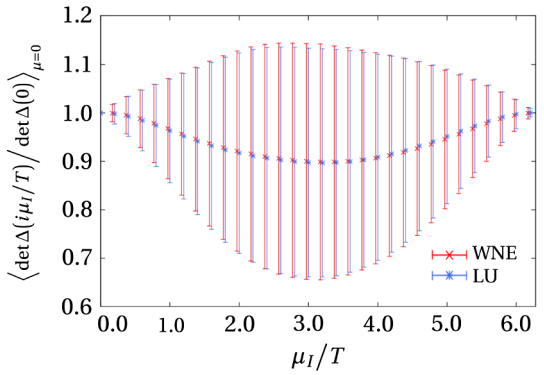

FIG. 10. Pure imaginary chemical potential dependence of fermion determinants. Red and blue points are calculated by the winding number expansion with 16 noise vectors and LU decomposition, respectively.

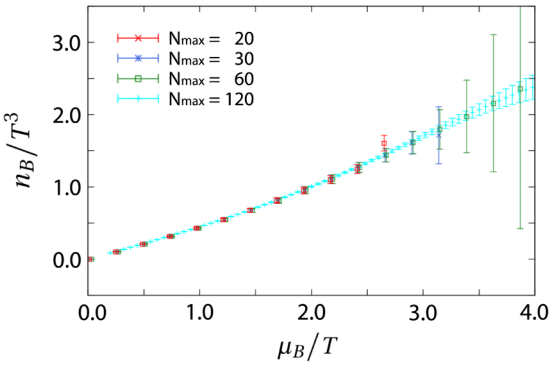

FIG. 11. The baryon number density as a function of its real baryon chemical potential for several $N_{\max}$. Here, $N_{\max}$ indicates the truncation of the fugacity expansion in Eq. (A1). Also, $\beta = 1.90$ $(T/T_c = 1.08)$. The line with $N_{\max} = 120$ corresponds to the data in Fig. 6.

APPENDIX C: VALIDITY OF NOISE METHOD FOR CALCULATION OF TRACE

As explained in Sec. III C 1, we adopt a noise method to calculate the trace in Eq. (11). Therefore, the problem we have to verify is if fermion determinants obtained through the noise method are consistent with these calculated exactly by LU decomposition.

To check this, we calculate fermion determinants at various values of purely imaginary chemical potential using both a noise method and LU decomposition at $T/T_c = 1.08$ as a test.

In this analysis, we adopt the RG-improved gauge action and the standard Wilson fermion action on a 4^4 lattice, and fermion determinants are averaged over 100 configurations generated at $\mu = 0$. We use 16 noise vectors for the traces appearing in the winding number expansion. Figure 10 shows that the noise method can produce consistent results with these obtained by LU decomposition within a range of statistical errors. Consequently, our winding number

expansion method with noise vectors works reliably in our analyses.

As $|n|$ increases, W_n values drop rapidly, and their accuracy is, in general, worse since we use the stochastic method. The contribution of $W_n\xi^n$ for large $|n|$ with $\xi = \exp(\mu/T)$ becomes prominent for real μ. Therefore, physical quantities investigated in this paper may suffer from noisy W_n with large $|n|$. In order to see the limitation of the canonical approach, we show in Fig. 11 the behavior of the baryon number density at real μ regions when changing $N_{\max}$ in Eq. (A1). The terms $W_n\xi^n$ for $|n| \geq N_{\max} + 1$ are set to be zero. By this test, therefore, we can see the effects of W_n with large $|n|$. We see that for $\mu_B/T < 3$, the result is not sensitive for $N_{\max}$, namely, in these regions, W_n values with large $|n|$ do not contribute physical quantity.

[1] K. Fukushima and T. Hatsuda, Rep. Prog. Phys. **74**, 014001 (2011).
[2] A. Hasenfratz and D. Toussaint, Nucl. Phys. **B371**, 539 (1992).
[3] A. Nakamura, S. Oka, and Y. Taniguchi, *Proc. Sci.*, LATTICE2014 (2015) 198.
[4] A. Nakamura, S. Oka, and Y. Taniguchi, J. High Energy Phys. 02 (2016) 054.
[5] Z. Fodor and S. D. Katz, J. High Energy Phys. 03 (2002) 014.
[6] C. R. Alton, S. Ejiri, S. J. Hands, O. Kaczmarek, F. Karsch, E. Laermann, Ch. Schmidt, and L. Scorzato, Phys. Rev. D **66**, 074507 (2002).
[7] I. M. Barbour and Z. A. Sabeur, Nucl. Phys. **B342**, 269 (1990).
[8] X.-F. Meng, A. Li, A. Alexandru, and K.-F. Liu, *Proc. Sci.*, LATTICE2008 (2008) 032.
[9] C. Gattringer and H.-P. Schadler, Phys. Rev. D **91**, 074511 (2015).
[10] J. Danzer and C. Gattringer, Phys. Rev. D **78**, 114506 (2008).
[11] K. Nagata and A. Nakamura, Phys. Rev. D **82**, 094027 (2010).
[12] A. Alexandru and U. Wenger, Phys. Rev. D **83**, 034502 (2011).
[13] K. Nagata and A. Nakamura, J. High Energy Phys. 04 (2012) 092.
[14] P. de Forcrand, *Proc. Sci.*, LATTICE2009 (2009) 010.
[15] A. Nakamura, Phys. Lett. **149B**, 391 (1984).
[16] A. Nakamura and K. Nagata, Prog. Theor. Exp. Phys. **2016**, 033D01 (2016).
[17] C. N. Yang and T. D. Lee, Phys. Rev. **87**, 404 (1952); T. D. Lee and C. N. Yang, Phys. Rev. **87**, 410 (1952).
[18] Y. Iwasaki, Report No. UTHEP-118 (1983).
[19] B. Sheikholeslami and R. Wohlert, Nucl. Phys. **B259**, 572 (1985).
[20] A. Roberge and N. Weiss, Nucl. Phys. **B275**, 734 (1986).
[21] P. de Forcrand and S. Kratochvila, Nucl. Phys. B, Proc. Suppl. **153**, 62 (2006).
[22] S. Ejiri, Y. Maezawa, N. Ukita, S. Aoki, T. Hatsuda, N. Ishii, K. Kanaya, and T. Umeda (WHOT-QCD Collaboration), Phys. Rev. D **82**, 014508 (2010).
[23] R. Fukuda, A. Nakamura, S. Oka, S. Sakai, A. Suzuki, and Y. Taniguchi, *Proc. Sci.*, LATTICE2015 (2015) 208.
[24] D. M. Smith, http://myweb.lmu.edu/dmsmith/FMLIB.html.
[25] P. de Forcrand and O. Philipsen, Nucl. Phys. **B642**, 290 (2002).
[26] A. Li, A. Alexandru, and K. F. Liu, Phys. Rev. D **84**, 071503 (2011).
[27] A. Alexandru, M. Faber, I. Horvath, and K. F. Liu, Phys. Rev. D **72**, 114513 (2005).
[28] A. Li, A. Alexandru, K. F. Liu, and X. Meng, Phys. Rev. D **82**, 054502 (2010).
[29] A. Alexandru, C. Gattringer, H.-P. Schadler, K. Splittorff, and J. J. M. Verbaarschot, Phys. Rev. D **91**, 074501 (2015).
[30] C. Gattringer and H.-P. Schadler, Phys. Rev. D **91**, 074511 (2015).